Joint cmWave-based Multiuser Positioning and Network Synchronization in Dense 5G Networks

Mike Koivisto*, Jukka Talvitie*, Mário Costa†, Kari Leppänen†, and Mikko Valkama*
* Laboratory of Electronics and Communications Engineering, Tampere University of Technology, Finland
† Huawei Technologies Oy (Finland) Co., Ltd, Finland R&D Center
Email: mike.koivisto@tut.fi

***Abstract*—The expected fifth generation (5G) networks allow for highly accurate direction of arrival and time of arrival (ToA) estimation, thus providing a convenient environment for device positioning, if designed properly. However, utilizing ToA measurements for positioning requires a tight synchronization not only between the target devices but also among the network elements. In this paper, we propose a joint positioning and synchronization solution building on the premises of the envisioned cmWave-based 5G ultra-dense networks and time-varying clock models. In addition to device location estimates, also relative clock offsets and skews are estimated and tracked within the proposed extended Kalman filter based solutions, which can be further used by a network operator in synchronizing the active network elements and devices within the network. Based on extensive simulations and numerical evaluations, accurate positioning performance can be achieved while tracking the clock parameters under time-varying clock errors.**

***Index Terms*—5G networks, extended Kalman filter, positioning, synchronization, tracking, ultra dense networks**

I. Introduction

In contrast to the earlier and existing mobile generations where positioning has only been an add-on feature, future fifth generation (5G) radio networks are expected to be able to provide $1\,\mathrm{m}$ positioning accuracy in 80% of the time in both outdoor and indoor environments [1], or even better accuracy for the most demanding use cases like autonomous vehicles, for instance [2]. Such an envisioned positioning accuracy substantially outperforms existing positioning techniques such as global navigation satellite system (GNSS)-based solutions where the accuracy is typically around $5\,\mathrm{m}$ [3, Chapter 8.5], observed time difference of arrival (OTDoA)-based positioning in LTE, where the positioning accuracy is usually tens of meters [4], and WLAN or Bluetooth-based positioning solutions where an accuracy of around 2-$5\,\mathrm{m}$ can be usually reached [5].

In order to meet the expected and demanding requirements of future 5G communication networks, e.g., in terms of peak data-rate, capacity and latency, it is widely expected that networks will be deployed with a high spatial density of transmission and reception points (TRPs) [6], [7]. Such a property together with a large bandwidth, which in turn enables highly accurate time of arrival (ToA) estimation from the received signal, are convenient properties for not only future demanding communications but also positioning purposes. Moreover, large antenna arrays and smart antenna solutions are able to estimate direction of arrival (DoA) angles from the received signals with a very high accuracy [8], [9]. Building on the premises of the expected ultra-dense cmWave-based 5G networks, we propose an efficient joint positioning and network synchronization approach where we take advantage of the expected 5G properties including high density of mobile devices. In addition to the acquired valuable synchronization information which can be utilized by a network operator for even improved communications, the obtained location information can be further used in radio resource management and to assist mmWave-based communications by designing the necessary beamformers [10], for instance.

Joint positioning and synchronization is a relatively widely explored theme in the existing literature. Solutions for joint positioning and synchronization are proposed in a cooperative or non-cooperative manner, e.g., in [11]–[13]. However, in these approaches, static networks are assumed which may not be a practical assumption in multiuser networks with rather dynamic target objects. In addition, these solutions as well as the 5G positioning and synchronization related work, e.g., in [8], consider at least one reference node with a synchronous clock. Selecting a feasible reference node may, in turn, be challenging or impractical in dynamic multiuser networks. Hence, in this paper, we propose a joint extended Kalman filter (EKF)-based positioning and synchronization solution which is able to estimate and track not only the location of the user equipments (UEs) but also the relative clock parameters between the active UEs and TRPs as well as between the TRPs without assuming a reference-time from a reference TRP.

The rest of the paper is organized as follows. First, we present the considered network structure together with the assumed channel and clock models in Section II. In Section III, general equations of the maximum likelihood (ML) and EKF estimation solutions are shortly presented before revising and applying them in the actual positioning and synchronization solution in Section IV. Thereafter, the simulation environment and the assumed numerology are presented in Section V before the results from simulations, and numerical evaluations, are presented and discussed in Section VI. Finally, we conclude the paper in Section VII.

II. System Model

In the considered multiuser ultra-dense network (UDN), we denote the set of TRP and active UE indices as $\mathcal{R}$ and

This work was supported by the Doctoral Program of the President of Tampere University of Technology, the Tuula and Yrjö Neuvo Fund, the Nokia Foundation, and the Finnish Funding Agency for Technology and Innovation (Tekes), under the projects "TAKE-5: 5th Evolution Take of Wireless Communication Networks", and "WIVE: Wireless for Verticals".

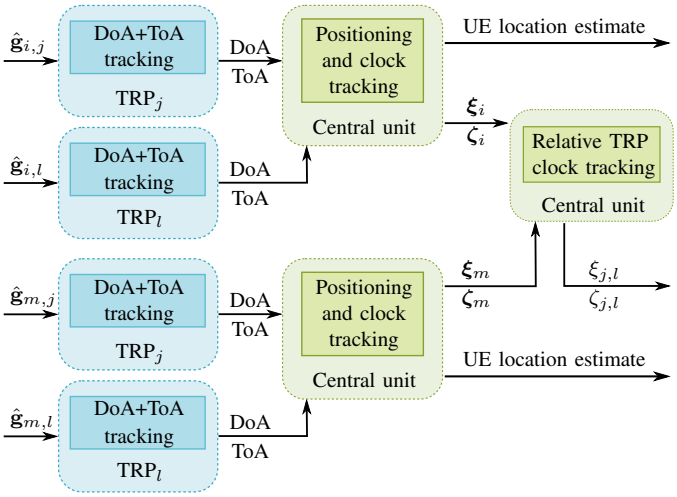

Fig. 1: A simplified visualization of the proposed positioning and synchronization method consisting of cascaded tracking solutions. In the first step, the DoAs and ToAs are estimated for each active UE [8], and the obtained estimates are then fused into location and clock parameter estimates. Finally, the clock offset and skew estimates between the UE and LoS-TRPs are used in estimating the relative clock parameters between the TRP-pair.

$\mathcal{U}$, respectively. Each UE is assumed to be equipped with a dipole antenna and located at an unknown position $\mathbf{p}_i = [x_i, y_i, z_i]^{\mathrm{T}}$, $\forall i \in \mathcal{U}$, whereas each TRP, at a known location $\mathbf{p}_j = [x_j, y_j, z_j]^{\mathrm{T}}$, $\forall j \in \mathcal{R}$, are assumed to be equipped with an antenna array and certain baseband unit (BBU). In general, each UE transmits periodic uplink pilot signals in the form of orthogonal frequency division multiplexing (OFDM) waveforms in an orthogonal frequency division multiple access (OFDMA) manner. These uplink pilot signals, which are anyway exchanged between the UEs and TRPs in order to acquire the necessary channel information, are then received by the line of sight (LoS)-TRPs. In particular, the LoS-probability in such UDNs is relatively high and therefore, it is likely that a given UE is in LoS-condition towards one or several TRPs most of the time. In this paper, we assume that each TRP is able to determine whether it is in LoS-condition towards the transmitting UE or not.

Thereafter, each LoS-TRP estimates the DoAs and ToAs from the received pilot signals individually for all active UEs as proposed in [8], and these estimates are then gathered and fused from all the LoS-TRPs into UE location estimates and corresponding clock parameter estimates at a central entity of the network. In contrast to, e.g., [8] where the absolute clock offsets and skews are tracked assuming a reference TRP, we seek to estimate the relative offsets and skews between UEs and active LoS-TRPs, thus allowing us to relax the assumption about having a reference time from a reference TRP. In the proposed positioning and synchronization solution the obtained relative clock variables are further used for estimating and tracking the relative clock errors between the active TRPs which can then be used to synchronize the corresponding TRPs within a network by a network operator. The different phases of the proposed solution are depicted in Fig. 1.

A. Channel model

In this paper, we utilize the estimated uplink single-input multiple-output (SIMO) channel response information in estimating and tracking the directional and temporal channel parameters of the LoS-path in a similar manner as in [8]. We exploit the following model for the multiantenna-multicarrier uplink SIMO channel response $\hat{\mathbf{g}}_{i,j} \in \mathbb{C}^{\mathcal{M}_{\mathrm{Rx}}\mathcal{M}_f \times 1}$ between the i^{th} UE and j^{th} LoS-TRP [14]

$$\hat{\mathbf{g}}_{i,j} = \mathbf{B}_j(\vartheta_{i,j}, \varphi_{i,j}, \tau_{i,j})\gamma + \mathbf{w} \tag{1}$$

where $\tau_{i,j}$, and $\varphi_{i,j}$ and $\vartheta_{i,j}$ denote the ToA[1], azimuth and elevation DoA angles between a given UE and LoS-TRP, respectively. Furthermore, $\mathcal{M}_{\mathrm{Rx}}$ denotes the number of antenna elements at TRP, $\mathcal{M}_f$ denotes the number of subcarriers, and $\mathbf{B}_j(\vartheta_{i,j}, \varphi_{i,j}, \tau_{i,j}) \in \mathbb{C}^{\mathcal{M}_{\mathrm{Rx}}\mathcal{M}_f \times 2}$ is the polarimetric antenna array response and it is given in terms of effective aperture distribution functions (EADFs) [14]. Finally, $\gamma \in \mathbb{C}^{2\times 1}$ denotes the unknown complex path-weights of the LoS-path and $\mathbf{w}$ is complex-circular zero-mean Gaussian noise with variance σ_w^2. We exploit the model in (1) for highly accurate DoA and ToA estimation at the LoS-TRPs using the EKF-based solution proposed in [8].

B. Clock model

In order to model clocks at UEs and TRPs as realistically as possible, we consider time-varying clock offsets in both transmitting UEs and receiving LoS-TRPs. In this paper, we denote the clock offset and skew of the i^{th} UE or TRP at time-instant n as $\rho_i[n]$ and $\alpha_i[n]$, respectively. As shown, e.g., in [15], the evolution of a given time-varying clock offset can be described by a first-order auto-regressive model

$$\begin{aligned} \rho_i[n] &= \rho_i[n-1] + \Delta t \alpha_i[n-1] \\ \alpha_i[n] &= \beta \alpha_i[n-1] + u[n], \end{aligned} \tag{2}$$

where $|\beta| < 1$, Δt is the time-interval between the consecutive time-instants $n-1$ and n, and $u[n] \sim \mathcal{N}(0, \sigma_u^2)$ denotes a zero-mean Gaussian noise in the clock skew. In particular, the standard deviation of the noise term can be interpreted as a measure of the oscillator stability of a given clock.

In order to synchronize the considered network without using a reference time from a reference TRP, we define variables $\xi_{i,j}[n]$ and $\zeta_{i,j}[n]$ which describe the relative clock offset and skew between the i^{th} transmitting UE and j^{th} receiving LoS-TRP, respectively. Using the clock offset evolution model in (2) and the definitions above, we can write a model for the time-varying relative clock offset $\xi_{i,j}[n]$ as

$$\begin{aligned} \xi_{i,j}[n] &\triangleq \rho_j[n_j] - \rho_i[n_i] \\ &\approx \xi_{i,j}[n-1] + \Delta t \zeta_{i,j}[n-1] \\ \zeta_{i,j}[n] &\triangleq \alpha_j[n_j] - \alpha_i[n_i] \\ &= \beta \zeta_{i,j}[n-1] + u'[n] \end{aligned} \tag{3}$$

where n_j and n_i denote the reception and transmission time-instances of the j^{th} LoS-TRP and i^{th} UE, respectively. Here, a

[1]Actually, τ denotes a time-delay, whereas the actual ToA can be obtained from the delay by taking into account the clock of the receiving TRP.

small approximation is required, since we can actually only measure the relative offset between the UE at its transmission time and the TRP when it receives the signal. However, such an approximation does not have a significant impact in the result and is used more due to the notational consistency. Using the definition in (3) and the model in (2), we can express the relative offset between the j^{th} and l^{th} LoS-TRP $\xi_{j,l}[n]$ as

$$\begin{aligned}\xi_{j,l}[n] &\triangleq \rho_l[n_l] - \rho_j[n_j] = \xi_{i,l}[n] - \xi_{i,j}[n] \\ \zeta_{j,l}[n] &\triangleq \alpha_l[n_l] - \alpha_j[n_j] = \zeta_{i,l}[n] - \zeta_{i,j}[n],\end{aligned} \tag{4}$$

which can be then used to measure the relative clock offsets and skews between a given TRP-pair and further synchronize the TRPs within the considered network.

III. Estimation and Bayesian Filtering

In the proposed positioning and synchronization solution we utilize an EKF based estimation and tracking method which further employs an ML estimate in initializing the actual EKF. Therefore, we shortly present in this section the general ML and EKF equations which are then applied in Section IV. Throughout this paper, we denote the state vector of the system and the obtained measurements at a time-instant n as $\mathbf{x}[n]$ and $\mathbf{y}[n]$, respectively. We further assume that the transition between two consecutive states obeys a linear state model and the state of the system is related to the measurements through a non-linear measurement model, which can be written as

$$\mathbf{x}[n] = \mathbf{F}[n]\mathbf{x}[n-1] + \mathbf{v}[n] \tag{5}$$

$$\mathbf{y}[n] = \mathbf{h}(\mathbf{x}[n]) + \mathbf{u}[n], \tag{6}$$

where $\mathbf{v}[n] \sim \mathcal{N}(0, \mathbf{Q}[n])$ is a zero-mean Gaussian process noise and $\mathbf{u}[n] \sim \mathcal{N}(0, \mathbf{R}[n])$ is a Gaussian measurement model noise term.

A. Maximum likelihood (ML) estimation

One widely used estimation technique is the ML estimation that consists in maximizing the assumed likelihood function of the measurements. Considering the measurement model in (6), and assuming a deterministic parameter $\mathbf{x}[n]$, the maximum likelihood estimation problem can be formulated in a probabilistic form as a product of N conditionally independent measurements as [16]

$$\hat{\mathbf{x}}[n] = \underset{\mathbf{x}[n]}{\operatorname{argmax}} \prod_{j=1}^{N} p\left(\mathbf{y}_j[n] \middle| \mathbf{x}[n]\right), \tag{7}$$

where $\hat{\mathbf{x}}[n]$ is the ML estimator at a given time-instant. In this paper, we employ an iterative quasi-Newton method for solving (7). Furthermore, we can estimate the uncertainty of the obtained ML estimate by employing the observed Fisher information matrix (FIM) of the measurement model such that

$$\hat{\mathbf{P}}[n] = (\mathbf{J}_{\mathbf{x}}(\hat{\mathbf{x}}[n])^{\mathrm{T}}\mathbf{J}_{\mathbf{x}}(\hat{\mathbf{x}}[n]))^{-1}, \tag{8}$$

where the Jacobian matrix $\mathbf{J}$ is evaluated at $\mathbf{x} = \hat{\mathbf{x}}[n]$ such as

$$\mathbf{J}_{\mathbf{x}}(\hat{\mathbf{x}}[n]) = \left.\frac{\partial \mathbf{h}(\mathbf{x})}{\partial \mathbf{x}^{\mathrm{T}}}\right|_{\mathbf{x}=\hat{\mathbf{x}}[n]}. \tag{9}$$

Due to the fact that the ML estimator as such does not take into account any prior knowledge about the considered system, the DoA-only ML estimator is used in initializing the state vector for more extensive positioning and synchronization procedures. In the numerical evaluations presented in Section VI we, however, demonstrate also the positioning performance of the ML approach compared to the proposed EKF-based approaches.

B. Extended Kalman filter (EKF)

The EKF is a well-known Bayesian filtering method where non-linear system models are linearized using Taylor first-order approximations around the a priori mean, after which general Kalman filter (KF) equations can be applied. Assuming models (5)-(6) and knowledge about the initial distribution, the a priori mean $\hat{\mathbf{x}}^{-}[n]$ and covariance $\hat{\mathbf{P}}^{-}[n]$ can be evaluated using the prediction step equations

$$\hat{\mathbf{x}}^{-}[n] = \mathbf{F}[n]\hat{\mathbf{x}}^{+}[n-1] \tag{10}$$

$$\hat{\mathbf{P}}^{-}[n] = \mathbf{F}[n]\hat{\mathbf{P}}^{+}[n-1]\mathbf{F}[n]^{\mathrm{T}} + \mathbf{Q}[n]. \tag{11}$$

The obtained a priori estimates can be then updated using the available measurements in the update step of the EKF as

$$\mathbf{K}[n] = \hat{\mathbf{P}}^{-}[n]\mathbf{H}[n]^{\mathrm{T}}(\mathbf{H}[n]\hat{\mathbf{P}}^{-}[n]\mathbf{H}[n]^{\mathrm{T}} + \mathbf{R}[n])^{-1} \tag{12}$$

$$\hat{\mathbf{x}}^{+}[n] = \hat{\mathbf{x}}^{-}[n] + \mathbf{K}[n](\mathbf{y}[n] - \mathbf{h}(\hat{\mathbf{x}}^{-}[n])) \tag{13}$$

$$\hat{\mathbf{P}}^{+}[n] = (\mathbf{I} - \mathbf{K}[n]\mathbf{H}[n])\hat{\mathbf{P}}^{-}[n], \tag{14}$$

where $\hat{\mathbf{x}}^{+}[n]$ and $\hat{\mathbf{P}}^{+}[n]$ are the a posteriori mean and covariance matrix, respectively, and $\mathbf{H}[n] \triangleq \mathbf{J}_{\mathbf{x}}(\hat{\mathbf{x}}^{-}[n])$ is the Jacobian matrix of the non-linear measurement model evaluated at the a priori mean.

IV. Joint Positioning and Synchronization EKF

As shortly described in Section II, and illustrated in Fig. 1, after obtaining the DoA and ToA measurements, we seek to estimate and track not only the location of the UEs but also the relative clock offsets and skews between the UEs and active LoS-TRPs before estimating the relative clock offsets and skews between the active TRP-pairs. Assuming a constant acceleration motion model and the clock models in (3), we can write the state vector $\mathbf{x}[n] \in \mathbb{R}^{9+2N_i \times 1}$ for the i^{th} UE as

$$\mathbf{x}_i[n] = \left[\mathbf{p}_i^{\mathrm{T}}[n], \mathbf{v}_i^{\mathrm{T}}[n], \mathbf{a}_i^{\mathrm{T}}[n], \boldsymbol{\xi}_i^{\mathrm{T}}[n], \boldsymbol{\zeta}_i^{\mathrm{T}}[n]\right]^{\mathrm{T}}, \tag{15}$$

where the three-dimensional location, velocity and acceleration of the UE are given as

$$\mathbf{p}_i[n] = [x_i[n], y_i[n], z_i[n]]^{\mathrm{T}} \tag{16}$$

$$\mathbf{v}_i[n] = [v_{x_i}[n], v_{y_i}[n], v_{z_i}[n]]^{\mathrm{T}} \tag{17}$$

$$\mathbf{a}_i[n] = [a_{x_i}[n], a_{y_i}[n], a_{z_i}[n]]^{\mathrm{T}}, \tag{18}$$

respectively, and relative clock offsets and skews between the i^{th} UE and all the receiving LoS-TRPs are given as

$$\boldsymbol{\xi}_i[n] = [\xi_{i,1}[n], \xi_{i,2}[n], \ldots, \xi_{i,N_i}[n]]^{\mathrm{T}} \in \mathbb{R}^{N_i \times 1} \tag{19}$$

$$\boldsymbol{\zeta}_i[n] = [\zeta_{i,1}[n], \zeta_{i,2}[n], \ldots, \zeta_{i,N_i}[n]]^{\mathrm{T}} \in \mathbb{R}^{N_i \times 1}, \tag{20}$$

where N_i is the number of active LoS-TRPs for the i^{th} UE. The corresponding state transition matrix $\mathbf{F}[n] \in \mathbb{R}^{9+2N_i \times 9+2N_i}$ and state noise covariance matrix $\mathbf{Q}[n] \in \mathbb{R}^{9+2N_i \times 9+2N_i}$ can be thus written for the considered system as

$$\mathbf{F}[n] = \begin{bmatrix} \mathbf{I}_{3\times3} & \Delta t\mathbf{I}_{3\times3} & \frac{\Delta t^2}{2}\mathbf{I}_{3\times3} & \mathbf{0}_{3\times2N_i} \\ \mathbf{0}_{3\times3} & \mathbf{I}_{3\times3} & \Delta t\mathbf{I}_{3\times3} & \mathbf{0}_{3\times2N_i} \\ \mathbf{0}_{3\times3} & \mathbf{0}_{3\times3} & \mathbf{I}_{3\times3} & \mathbf{0}_{3\times2N_i} \\ \mathbf{0}_{2N_i\times3} & \mathbf{0}_{2N_i\times3} & \mathbf{0}_{2N_i\times3} & \mathbf{A} \end{bmatrix}$$

$$\mathbf{Q}[n] = \begin{bmatrix} \frac{\sigma_a^2\Delta t^5}{20}\mathbf{I}_{3\times3} & \frac{\sigma_a^2\Delta t^4}{8}\mathbf{I}_{3\times3} & \frac{\sigma_a^2\Delta t^3}{6}\mathbf{I}_{3\times3} & \mathbf{0}_{3\times2N_i} \\ \frac{\sigma_a^2\Delta t^4}{8}\mathbf{I}_{3\times3} & \frac{\sigma_a^2\Delta t^3}{3}\mathbf{I}_{3\times3} & \frac{\sigma_a^2\Delta t^2}{2}\mathbf{I}_{3\times3} & \mathbf{0}_{3\times2N_i} \\ \frac{\sigma_a^2\Delta t^3}{6}\mathbf{I}_{3\times3} & \frac{\sigma_a^2\Delta t^2}{2}\mathbf{I}_{3\times3} & \sigma_a^2\Delta t\mathbf{I}_{3\times3} & \mathbf{0}_{3\times2N_i} \\ \mathbf{0}_{2N_i\times3} & \mathbf{0}_{2N_i\times3} & \mathbf{0}_{2N_i\times3} & \mathbf{D} \end{bmatrix}, \quad (21)$$

where σ_a^2 denotes the variance of the acceleration noise. Furthermore, the sub-matrices $\mathbf{A}$ and $\mathbf{D}$ in (21) are defined as

$$\mathbf{A} = \begin{bmatrix} 1 & \Delta t \\ 0 & \beta \end{bmatrix} \otimes \mathbf{I}_{N_i\times N_i} \in \mathbb{R}^{2N_i\times2N_i} \quad (22)$$

$$\mathbf{D} = \begin{bmatrix} \frac{\sigma_\eta^2\Delta t^3}{3} & \frac{\sigma_\eta^2\Delta t^2}{2} \\ \frac{\sigma_\eta^2\Delta t^2}{2} & \sigma_\eta^2\Delta t \end{bmatrix} \otimes \mathbf{I}_{N_i\times N_i} \in \mathbb{R}^{2N_i\times2N_i}, \quad (23)$$

where $\otimes$ and σ_η^2 denotes the Kronecker product and variance of the clock skew process noise, respectively.

In the proposed positioning and synchronization EKF, we fuse the DoA and ToA measurements from all the LoS-TRPs into UE location and relative clock parameter estimates. For a given UE, we denote the augmented measurement model function as $\mathbf{h}(\mathbf{x}_i[n]) = [\mathbf{h}_1(\mathbf{x}_i[n])^{\mathrm{T}}, \ldots, \mathbf{h}_{N_i}(\mathbf{x}_i[n])^{\mathrm{T}}]^{\mathrm{T}}$, where $\mathbf{h}_j(\mathbf{x}_i[n]),\ \forall j = 1, \ldots, N_i$ is defined as

$$\mathbf{h}_j(\mathbf{x}_i[n]) = \begin{bmatrix} \text{atan}_2\left(y_i[n] - y_j,\ x_i[n] - x_j\right) \\ \text{atan}_2\left(z_i[n] - z_j,\ \|\mathbf{p}_i[n] - \mathbf{p}_j\|_{2\text{D}}\right) \\ \frac{\|\mathbf{p}_i[n]-\mathbf{p}_j\|}{c} + \xi_{i,j}[n] \end{bmatrix}, \quad (24)$$

where c is the speed of light, $\|\cdot\|_{2\text{D}}$ denotes a 2D distance on the xy-plane, and atan_2 denotes a multi-valued inverse tangent function. Furthermore, we denote the augmented measurement vector as $\mathbf{y}_i[n] = [\mathbf{y}_1^{\mathrm{T}}[n], \ldots, \mathbf{y}_{N_i}^{\mathrm{T}}[n]]^{\mathrm{T}}$ and the corresponding noise covariance matrix as $\mathbf{R}_i[n] = \text{blkdiag}(\mathbf{R}_1[n], \ldots, \mathbf{R}_{N_i}[n])$, where the measurement vector and noise covariance matrix obtained at the j^{th} LoS-TRP are denoted as $\mathbf{y}_j[n] = [\varphi_{i,j}[n], \vartheta_{i,j}[n], \tau_{i,j}[n]]^{\mathrm{T}}$ and $\mathbf{R}_j[n]$, respectively.

However, the EKF with the model (24) may suffer from high non-linearity underneath the TRPs [17], and hence, we also adopt a circular statistics into the measurement model in terms of a von Mises-Fisher (VMF) distribution based approximation as proposed in [17]. In the proposed VMF-based approach, the DoA measurements are first mapped onto a unit sphere and, thus, the updated measurement vectors and model functions become

$$\mathbf{h}'_j(\mathbf{x}_i[n]) = \begin{bmatrix} \frac{\mathbf{p}_i[n]-\mathbf{p}_j}{\|\mathbf{p}_i[n]-\mathbf{p}_j\|} \\ \frac{\|\mathbf{p}_i[n]-\mathbf{p}_j\|}{c} + \xi_{i,j}[n] \end{bmatrix} \quad (25)$$

$$\mathbf{y}'_j[n] = [\mathbf{f}(\varphi_{i,j}[n], \vartheta_{i,j}[n])^{\mathrm{T}}, \tau_{i,j}[n]]^{\mathrm{T}} \in \mathbb{R}^{4\times1}, \quad (26)$$

Algorithm 1 Positioning and Network Synchronization EKFs

For every time-instant $n = 1, \ldots, T$

  For every active UE $i \in \mathcal{U}$

    1) Estimate $\mathbf{y}_j[n]$ and $\mathbf{R}_j[n]$ at individual LoS-TRPs $j = 1, \ldots, N_i$ as proposed in [8]
    2) Initialize the state and covariance of the UE using ML estimates (7) and distributions presented in Section V if necessary.
    3) Gather $\mathbf{y}_i[n]$ and $\mathbf{R}_i[n]$ from all the LoS-TRPs and estimate the UE location $\mathbf{p}_i[n]$ and clock parameters $\boldsymbol{\xi}_i[n]$ and $\boldsymbol{\zeta}_i[n]$ using the EKF and models proposed in Section IV.

  end

  For every active TRP-pair (j, l), where $j, l \in \mathcal{R}$

    4) Estimate the relative clock offsets and skews between the TRPs, i.e., $\xi_{j,l}[n]$ and $\zeta_{j,l}[n]$, respectively, using a KF and models in Section II.

  end

end

where $\mathbf{f}(\varphi, \vartheta) = [\cos(\vartheta)\cos(\varphi), \sin(\vartheta)\cos(\varphi), \sin(\varphi)]^{\mathrm{T}}$ is a function that maps the directional variables to a unit vector when the poles of the unit sphere are defined as in [17].

The updated DoA measurements are now VMF distributed as $\mathbf{f}(\varphi_{i,j}[n], \vartheta_{i,j}[n]) \sim \text{VMF}\left(\frac{\mathbf{p}_i[n]-\mathbf{p}_j}{\|\mathbf{p}_i[n]-\mathbf{p}_j\|}, \kappa_{\mathbf{u}[n]}\right)$, where

$$\text{VMF}(\mathbf{x}; \boldsymbol{\mu}, \kappa) = C_\kappa e^{\kappa\boldsymbol{\mu}^{\mathrm{T}}\mathbf{x}}, \quad (27)$$

where $\|\mu\| = 1$, $\kappa \geq 0$ is a concentration parameter and C_κ is a normalization constant [18, Ch. 9.3]. In the EKFs, it is however assumed that the noise terms should be Gaussian and therefore, we exploit an approximation for the VMF-based measurement model as

$$\mathbf{f}(\varphi_{i,j}[n], \vartheta_{i,j}[n]) \sim \mathcal{N}\left(\frac{\mathbf{p}_i[n] - \mathbf{p}_j}{\|\mathbf{p}_i[n] - \mathbf{p}_j\|}, \frac{1}{\kappa_{\mathbf{u}[n]}}\mathbf{I}_{3\times3}\right), \quad (28)$$

where $\kappa_{\mathbf{u}[n]}^{-1} \triangleq \max\{\sigma^2_{\varphi_{i,j}[n]}, \sigma^2_{\vartheta_{i,j}[n]}\}$ [17]. In the proposed VMF-based approach, the measurement model for the ToA is the same as that of (24). Throughout the rest of the paper, we denote the proposed positioning and synchronization EKF that utilizes the measurement model in (24) as Pos&Sync EKF and the one that exploits the models in (25) and (28) as Pos&Sync VMF-EKF. In order to ensure fast convergence of the proposed EKFs, we first estimate the initial location of a given UE using an ML estimate and observed FIM, by employing the equations presented in Section III. Such an initialization process provides sufficient initial guess for the initial location of the UE which in turn increases the synchronization performance in the beginning of the filtering compared to the approach in [8].

The third phase of the proposed approach contains estimation and tracking of the relative clock offsets and skews between the active TRP-pairs as illustrated in Fig. 1. In this final step, the obtained relative clock estimates between the UEs and active LoS-TRPs, i.e., $\boldsymbol{\xi}_i[n]$ and $\boldsymbol{\zeta}_i[n]$ $\forall i \in \mathcal{U}$ are fused into the relative clock offset and skew estimates of the TRP-pairs. Since

TABLE I: Simulation numerology

Parameter	Value
Carrier frequency	3.5 GHz
Subcarrier spacing	15 kHz
Number of pilot subcarriers	64
Effective bandwidth	4.8 MHz
Transmit power	10 dBm
Transmission time-interval	200 µs
TRP inter-site distance	50 m
Antenna height	7 m
Antenna model	Semi-spherical (22 patch-elements) [22]
Speed of a pedestrian UE	3-4 km/h
Speed of a vehicle UE	15-45 km/h

these clock variables also follows the considered clock models, we implement a simple KF for tracking the relative clock offsets and skews between the TRP-pairs using the first part of (4) as a linear measurement model. The proposed KF-based tracking is again beneficial because it provides not only sequential estimates for the clock variables but also valuable information about the uncertainty of the obtained estimates. However, other estimation solutions such as ML can be exploited in the final step of the proposed method as well. A simplified algorithm of the proposed positioning and synchronization EKF solutions is presented in Algorithm 1.

V. Simulation Environment

In order to demonstrate the performance of the proposed positioning and synchronization EKFs, simulations and numerical evaluations are carried out in the realistic outdoor METIS Madrid map environment [19]. In particular, the METIS map-based ray-tracing channel model is implemented, thus allowing for simulating the propagation environment as realistically as possible [20]. Furthermore, we model both pedestrian and vehicle UEs through 50 random trajectories on the map. The pedestrian UEs are assumed to move with a constant velocity along straight lines on the sidewalks, whereas the vehicle UEs are following a realistic acceleration model designed for the vehicles [21]. In addition, interfering UEs are placed on the map randomly 250 m away from a given UE with a density of 1000 interferers/km^2. The numerology regarding the physical channels and network, presented in Table I, are mainly stemming from the expected 5G numerology.

Furthermore, we draw the initial clock offsets and skews for both UEs and TRPs from the distributions $\mathcal{N}(0, (100\,\mu\text{s})^2)$ and $\mathcal{N}(25\,\text{ppm}, (20\,\text{ppm})^2)$, respectively, and we set the clock skew driving noise to $\sigma_u^2 = 4 \cdot 10^{-15}$. Such clock model values are stemming from the discussion in Section II and that of [8]. Moreover, we set the clock model parameter for the actual clocks as $\beta = 0.9998$, whereas in the EKFs, we use $\beta = 1$ for the sake of generality. For the implemented EKFs, we also set the process noise variances in (21) to $\sigma_a^2 = (0.01\,\text{m/s}^2)^2$ and $\sigma_\eta^2 = (1 \cdot 10^{-5})^2$. Finally, we gather DoA and ToA measurements from two closest LoS-TRPs and fuse them into UE location and clock estimates every 100 ms.

VI. Results

In the numerical evaluations, the positioning performance of the proposed Pos&Sync EKF and Pos&Sync VMF-EKF is compared to more classical DoA-only EKF, DoA-only VMF-EKF and DoA-only ML, where only DoA measurements are utilized for positioning purposes. Furthermore, we implement also an EKF, denoted as Pos&Clock EKF, for the scenario where the TRPs are assumed synchronous and only UE devices are assumed to have time-varying clock offsets. In addition to the positioning performance, we analyze also the synchronization performance of the proposed solutions under the considered asynchronous network. The obtained positioning and synchronization results are depicted in Figs. 2-3.

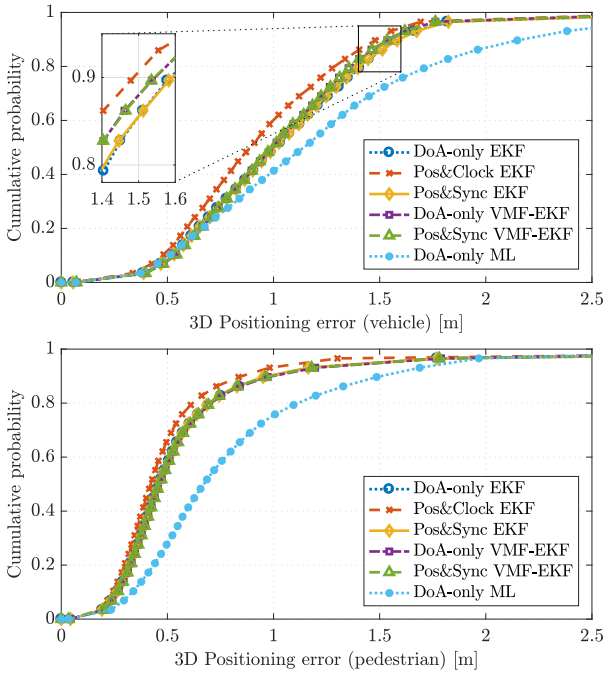

Fig. 2: 3D positioning CDFs for the considered positioning approaches for both vehicle (above) and pedestrian (below) UE scenarios.

Based on the obtained 3D positioning results visualized in Fig. 2 in terms of cumulative distribution functions (CDFs), a clear difference in positioning accuracy can be observed between pedestrian UEs and vehicle UEs as expected[2]. Such a difference is mainly due to the different speeds of the target types. Obviously, when tracking a target with a high speed without any velocity-related measurements, the positioning performance is usually worse compared to that of a target with a slower speed. We can also easily observe that the tracking solutions provide better positioning performance compared to the snapshot-based DoA-only ML solution, where the prior information of the state is not utilized in estimation. In pedestrian UE case, differences in the performance of the EKF-based solutions can not be clearly distinguished, whereas in vehicle UE positioning, the VMF-based EKFs slightly outperform the EKFs using the models (25). Such differences are even more visible in the considered UE scenarios when, e.g., cylindrical antenna models with worse geometry closer or underneath the TRPs are employed, which also emphasizes the role of VMF-based EKFs in positioning. It can be also

[2]A short video visualizing the positioning performance is available on-line at `http://www.tut.fi/5G/WCNC18/`

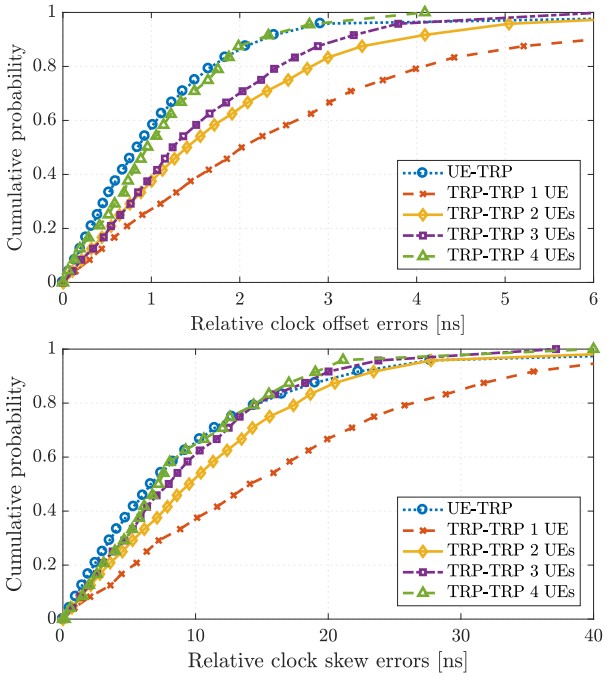

Fig. 3: Relative clock offset and skew tracking performance between UEs and LoS-TRPs, and between the TRP-pairs with different number of connecting UEs for the pedestrian UE case.

seen from the results in Fig. 2 that the ToA measurements are not significantly contributing to the positioning performance, and they are mainly used in synchronization in the considered filters. Despite the almost identical positioning performance of the different methods, the proposed DoA and ToA based approaches are able to provide also highly accurate clock estimates as a valuable by-product. Interestingly, the pedestrian UEs can be located with the accuracy of $1\,\mathrm{m}$ in $90\,\%$ of the situations, whereas better than $1.5\,\mathrm{m}$ accuracy can be achieved with the probability of $85\,\%$ for the considered vehicle UEs.

In addition to accurate positioning, not only the relative clock offsets and skews between the pedestrian UEs and active LoS-TRPs but also the clock offsets and skews between the active TRP-pairs can be estimated with an extremely high accuracy as illustrated in Fig. 3. As expected, the more there are UEs connecting a given TRP-pair the better is the relative clock offset and skew estimation performance between the TRPs due to noise reduction after averaging several measurements. Overall, better than $5\,\mathrm{ns}$ offset and $30\,\mathrm{ns}$ skew estimation accuracy can be achieved between the active TRP-pairs in more than $80\,\%$ of the cases even when only a single UE is connecting the TRP-pair. However, when four UEs are connected to the same TRP-pair, almost $4\,\mathrm{ns}$ relative clock offset estimation accuracy can be acquired in all situations.

VII. Conclusions

In this paper, we proposed a joint 3D device positioning and synchronization solution building on the premises of the expected cmWave-based 5G UDNs and realistic time-varying clock models. In addition to device location estimates, also relative clock offsets and skews are estimated and tracked in the proposed EKF based solutions, which can be further utilized by a network operator in synchronizing the active network elements and devices within the network. Based on extensive simulations and numerical evaluations, highly accurate positioning performance can be achieved while tracking the relative clock offsets and skews among the asynchronous devices and network elements.

References

[1] 3GPP TR 22.862, "Feasibility study on new services and markets technology enablers for critical communications; stage 1 (V14.1.0)," Sep. 2016. [Online]. Available: http://www.3gpp.org/DynaReport/22862.htm

[2] 5G-PPP, "5G automotive vision," Oct. 2015. [Online]. Available: https://5g-ppp.eu/wp-content/uploads/2014/02/5G-PPP-White-Paper-on-Automotive-Vertical-Sectors.pdf

[3] K. Borre, D. M. Akos, N. Bertelsen, P. Rinder, and S. H. Jensen, *A Software-Defined GPS and Galileo Receiver - A Single-Frequency Approach*. Birkhäuser Boston, 2007.

[4] J. Medbo, I. Siomina, A. Kangas, and J. Furuskog, "Propagation channel impact on LTE positioning accuracy: A study based on real measurements of observed time difference of arrival," in *Proc. IEEE PIMRC*, Sep. 2009, pp. 2213–2217.

[5] H. Liu, H. Darabi, P. Banerjee, and J. Liu, "Survey of Wireless Indoor Positioning Techniques and Systems," *IEEE Transactions on Systems, Man, and Cybernetics, Part C (Applications and Reviews)*, vol. 37, no. 6, pp. 1067–1080, Nov. 2007.

[6] N. Bhushan, J. Li, D. Malladi, R. Gilmore, D. Brenner, A. Damnjanovic, R. Sukhavasi, C. Patel, and S. Geirhofer, "Network densification: the dominant theme for wireless evolution into 5G," *IEEE Commun. Mag.*, vol. 52, no. 2, pp. 82–89, Feb. 2014.

[7] A. Dammann, R. Raulefs, and S. Zhang, "On prospects of positioning in 5G," in *Proc. IEEE International Conf. on Communication Workshop (ICCW)*, Jun. 2015, pp. 1207–1213.

[8] M. Koivisto, M. Costa, J. Werner, K. Heiska, J. Talvitie, K. Leppänen, V. Koivunen, and M. Valkama, "Joint device positioning and clock synchronization in 5G ultra-dense networks," *IEEE Trans. Wireless Commun.*, vol. 16, no. 5, May 2017.

[9] M. Koivisto, A. Hakkarainen, M. Costa, P. Kela, K. Leppänen, and M. Valkama, "High-Efficiency Device Positioning and Location-Aware Communications in Dense 5G Networks," *IEEE Communications Magazine*, vol. 55, no. 8, pp. 188–195, 2017.

[10] P. Kela, M. Costa, J. Turkka, M. Koivisto, J. Werner, A. Hakkarainen, M. Valkama, R. Jäntti, and K. Leppänen, "Location Based Beamforming in 5G Ultra-Dense Networks," in *2016 IEEE 84th Vehicular Technology Conference (VTC-Fall)*, Sep. 2016, pp. 1–7.

[11] A. Ahmad, E. Serpedin, H. Nounou, and M. Nounou, "Joint Node Localization and Time-Varying Clock Synchronization in Wireless Sensor Networks," *IEEE Transactions on Wireless Communications*, vol. 12, no. 10, pp. 5322–5333, Oct. 2013.

[12] B. Etzlinger, H. Wymeersch, and A. Springer, "Cooperative Synchronization in Wireless Networks," *IEEE Transactions on Signal Processing*, vol. 62, no. 11, pp. 2837–2849, Jun. 2014.

[13] O. Jean and A. Weiss, "Passive Localization and Synchronization Using Arbitrary Signals," *IEEE Trans. Signal Process.*, vol. 62, no. 8, pp. 2143–2150, Apr. 2014.

[14] A. Richter, "Estimation of radio channel parameters: Models and algorithms," Ph.D. dissertation, Ilmenau University of Technology, http://www.db-thueringen.de/servlets/DerivateServlet/Derivate-7407/ilm1-2005000111.pdf, 2005.

[15] H. Kim, X. Ma, and B. Hamilton, "Tracking low-precision clocks with time-varying drifts using Kalman filtering," *IEEE/ACM Trans. Netw.*, vol. 20, no. 1, pp. 257–270, Feb. 2012.

[16] S. Särkkä, *Bayesian filtering and smoothing*. Cambridge University Press, 2013.

[17] H. Nurminen, L. Suomalainen, S. Ali-Löytty, and R. Piché, "3D angle-of-arrival positioning using von Mises-Fisher distribution," Sep. 2017. [Online]. Available: http://adsabs.harvard.edu/abs/2017arXiv170902437N

[18] K. V. Mardia and P. E. Jupp, *Directional Statistics*. John Wiley & Sons, ltd, 2000.

[19] METIS, "D6.1 Simulation guidelines," Oct. 2013. [Online]. Available: https://www.metis2020.com/wp-content/uploads/deliverables/METIS_D6.1_v1.pdf

[20] METIS, "D1.4 Channel models," Feb. 2015. [Online]. Available: https://www.metis2020.com/wp-content/uploads/METIS_D1.4_v3.pdf

[21] R. Akcelik and D. C. Biggs, "Acceleration profile models for vehicles in road traffic," *Transportation Science*, no. 1, pp. 36–54, Feb. 1987.

[22] V. M. Kolmonen, J. Kivinen, L. Vuokko, and P. Vainikainen, "5.3-GHz MIMO radio channel sounder," *IEEE Transactions on Instrumentation and Measurement*, vol. 55, no. 4, pp. 1263–1269, Aug. 2006.